https://dx.doi.org/10.1016/j.bioadv.2022.212831

An anti-bacterial and anti-cancer fibrous membrane with multiple therapeutic effects for prevention of pancreatic cancer recurrence

Qiang Zhang, Yang Luo, Bo Liang, Di Suo, Shang Lyu, Yi Wang, Xin Zhao

Abstract

Adjuvant systemic chemotherapy with gemcitabine (GEM) is recognized as the standard of care to improve the prognosis of patients with resected pancreatic cancer (PC); however, it is greatly limited by poor absorption of chemotherapy agents. Moreover, surgical site infection and Gammaproteobacteria-induced GEM resistance further decrease the chemotherapy efficacy and increase the risk of recurrence and even mortality. Here, we develop an implantable anti-bacterial and anti-cancer fibrous membrane (AAFM) to inhibit PC recurrence in a well- coordinated manner. Our AAFM can be readily prepared via simple co-electrospinning of GEM and poly-L-lactic acid (PLLA) and subsequent tannic acid (TA)-mediated in-situ generation of silver nanoparticles (AgNPs). The resultant membrane presents highly porous fibrous morphology and appropriate mechanical performance. Most importantly, we find the surface-deposited TA/AgNP complexes can exert multiple therapeutic effects: (1) they can act as a fence to extend GEM diffusion route, achieving a sustained drug release; (2) they can fight the pathogenic microorganisms in the local microenvironment and prevent infectious complica- tions and alleviate Gammaproteobacteria-induced chemotherapy resistance; (3) they can combat residual cancer cells to synchronously strengthen the effectiveness of GEM-based chemotherapy. Altogether, our AAFM provides a proof-of-concept demonstration of the integrated anti-cancer and anti-bacterial strategy for enhanced therapeutic efficacy and will inspire the design of other high performance implants for prevention of tumor relapse.

1. Introduction

Pancreatic cancer (PC), also known as pancreatic ductal adenocarcinoma, is one of the most lethal solid malignancies in the world, with an overall 5-year survival rate of less than 10% [1,2]. Currently, surgical resection, especially the pancreaticoduodenectomy, remains the only potentially curative strategy to improve the prognosis of patients with advanced PC, but approximately 80% of these patients after surgery will eventually undergo cancer recurrence [3]. Numerous studies have now revealed the post-operative residual tumor cells or micro-tumors in the surgical margins constitute the primary reason for local tumor relapse [4,5]. To reduce the incidence of tumor recurrence, current standard of care is to implement adjuvant chemotherapy immediately after PC resection [6]. However, these chemotherapy agents are often administrated systemically via intravenous injection, which may lead to serious side effects and complications, significantly compromising the clinical outcomes [7,8]. In this respect, new treatments that can reduce the detrimental adverse effects of adjuvant chemotherapy while improving the clinical outcome of cancer therapy are highly sought after.

Nowadays, drug delivery systems that can release drugs in a controlled and sustained manner have been recognized as a favourable solution to enhance the efficacy of adjuvant chemotherapy [9]. In terms of the mechanisms and administration routes, such drug delivery systems can be roughly classified into two types: local and systemic treatments [4]. For systemic treatments, various cellular-based vehicles and synthetic nanocarriers are employed to load bioactive therapeutic molecules. Depending on the specific surface modification and the enhanced permeability and retention (EPR) effect, these systemic delivery systems can realize a targeted drug accumulation in tumor sites after intravenous injection [9]. Nevertheless, their preparation process is complicated, time-consuming, and difficult to control precisely, restraining the large-

scale production. Moreover, the cost of functionalization of these delivery systems may be too high to fulfil the requirements of clinical applications. More importantly, PC is characterized by a low blood supply compared with other types of cancers, in which most blood vessels are crushed and shut [10]. In addition to the reduced microvascular density after curative resection, it is troublesome for the accumulation of chemotherapy drugs in the PC tumors by EPR effect. Therefore, local delivery systems stand out since they can be implanted to the surgical site, enhance the local drug dosage, facilitate the sustained drug release administration, and minimize the harmful side effects to organs/tissues [9]. To date, diverse formulations and devices have been proposed including wafers [11], hydrogels [12] and fibers [13,14]. Among them, electrospun fibers have attracted great research attention in the recent decade owing to their facile fabrication, high drug loading ability, large specific surface area and 3D porous structure. By adjusting the electrospinning parameters (e.g., material composition and drug dose) and drug-loading methods (e.g., surface modification, blending, coaxial or emulsion), the release behavior of the encapsulated drugs can be well controlled [15]. Unfortunately, these local treatments based on the electrospun fibers may only have a single biofunction and only focus on the clearance of tumor cells without considering the prevention of other surgery-related complications, failing to balance curative effects and side effects during the long-term adjuvant chemotherapy. To further strengthen the efficacy of the post- operative adjuvant chemotherapy, it is desirable to orchestrate a variety of therapeutic strategies according to the unique tumor microenvironment, synchronously enhancing the tumor-killing effect, reducing side effects and preventing related complications. It has been reported that pancreaticobiliary surgery has a high risk of surgical site infection reaching 20%–40%, which is mainly due to the colonization of gut microorganisms during pancreatectomy [16,17]. Long-term follow-up studies have demonstrated that such infectious complication is closely related with poor overall survival, high recurrence rate, in-hospital death, and healthcare costs [16]. Moreover, a recent study published in Science revealed that Gammaproteobacteria, the most prevalent bacteria in the PC microenvironment, could ad hoc diminish the efficacy of gemcitabine (GEM, one of the standard first-line chemotherapeutic agents) and increase the chemoresistance by secreting cytidine deaminase to convert GEM into its inactive form, 20,20-difluorodeoxyuridine [18–20]. Consequently, we speculate that it may be a promising strategy to develop a drug delivery platform with strong inherent antibacterial activity, which can fight bacteria in the local microenvironment to avoid surgical site infection and reduce the risk of Gammaproteobacteria-induced GEM resistance, while continuously deliver chemotherapeutic agents to kill

the residual cancer cells.

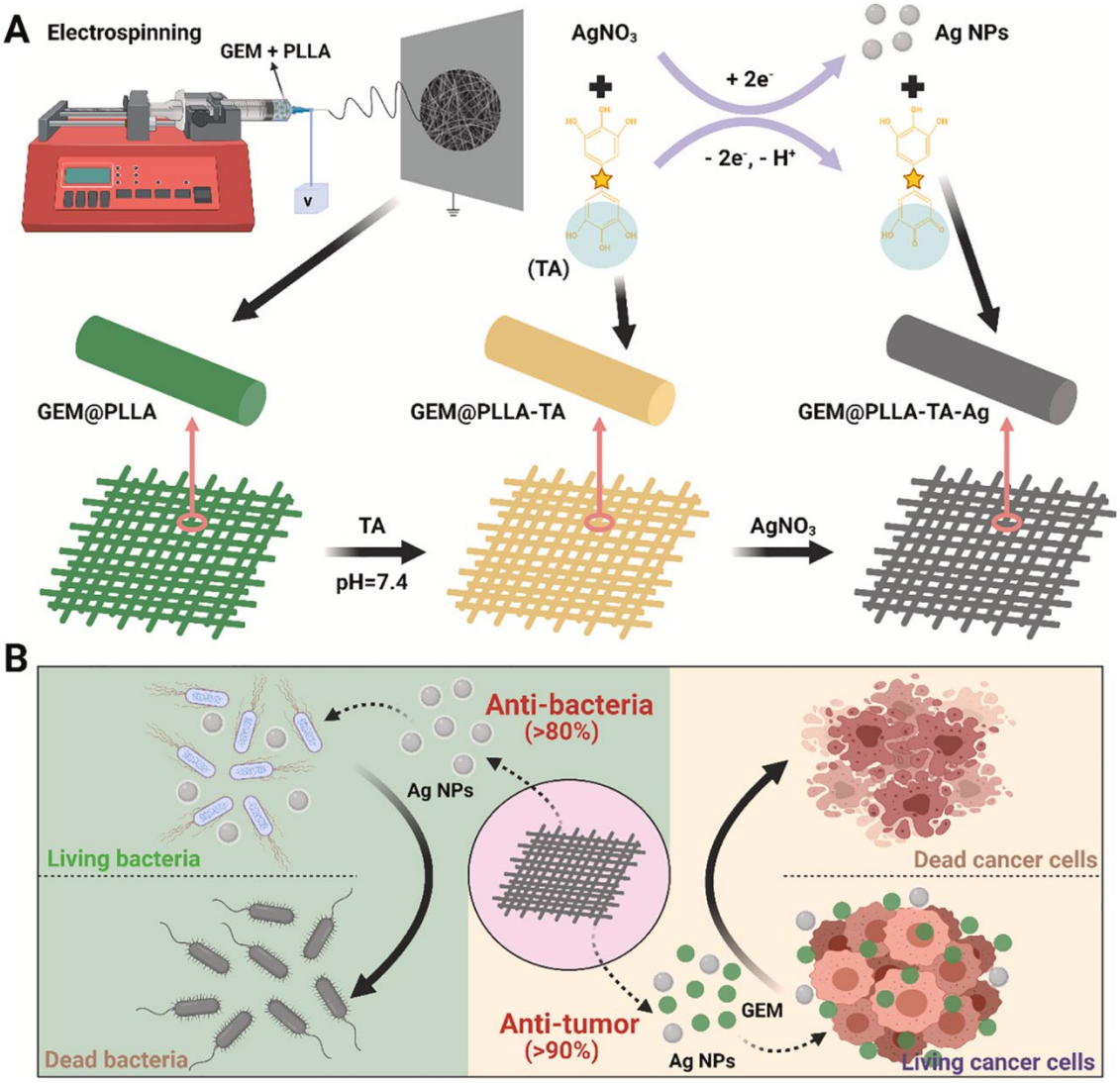

Fig. 1. Schematic illustration of the development of anti-bacterial and anti-cancer fibrous membranes (AAFM) for prevention of PC recurrence. (A) The preparation process of AAFM by co-electrospinning of GEM and PLLA and subsequent TA-mediated in-situ AgNP synthesis. TA forms a multi-functional coating on the PLLA fibers and then reduces the silver nitrate to AgNPs bound to the coating surface. (B) The resultant AAFM exhibits excellent anti-bacterial performances, which can prevent surgical site infection and combat Gammaproteobacteria to alleviate GEM resistance. Meanwhile, the release of AgNPs and GEM will synergistically eliminate the residual tumor cells, thereby effectively suppressing the local tumor recurrence after surgery. Figure created with BioRender.com.

Here, we prepare an implantable anti-cancer and anti-bacterial fibrous membrane (AAFM) via facile combination of the electro- spinning technology and dipping approach. First, a GEM-loaded fibrous membrane is fabricated by feasible blending electrospinning of GEM and poly-L-lactic acid (PLLA) (Fig. 1A). Subsequently, a simple tannic acid (TA)-mediated two-step dipping process is performed for in-situ synthesis of silver nanoparticles (AgNPs) onto electrospun fibers. Due to the superior good adhesive capacity, TA can form a multifunctional coating on the PLLA fibers and then reduce the silver nitrate to AgNPs tightly bound to the surface of TA coating [21]. The resultant electrospun fibers are expected to have multiple synergistic effects: (1) the surface- deposited TA/AgNP complexes work as an armour on the PLLA fibers, acting as a barrier to impede GEM diffusion and facilitate a sustained release pattern; (2) TA/AgNP complexes equip the system with excellent anti-bacterial performance, which is believed to reduce surgical

site infection rate and alleviate the GEM resistance; (3) the delivery system itself (i.e., PLLA-TA-Ag) exhibits superior inhibitory effects on tumor cell growth both in vitro and in vivo, and can work together with GEM to enhance the anti-tumor efficacy (Fig. 1B). In terms of these unique features, we envision that our AAFM will effectively prevent PC recurrence and prolong survival of the resected patients, holding great clinical potential for local PC therapy.

2. Material and methods

2.1. Preparation of the anti-bacterial and anti-cancer electrospun fibrous scaffolds

First, we prepared GEM-loaded PLLA electrospun membranes by blending GEM into the PLLA electrospun precursor solution prior to electrospinning. PLLA precursor solution at 20% (w/v) was obtained by adding 0.6 g PLLA into 3 mL hexafluoroisopropanol followed by constant stirring until complete dissolution. Then, different weights of GEM (90, 180, 360 mg) were added into the asprepared PLLA solution to obtain the electrospun solutions (named GEM1@PLLA, GEM2@PLLA, and GEM3@PLLA, respectively). During the electrospinning, the voltage was set to 15–20 kV, the receiving distance between the injector and collector was 20 cm, and the feed rate of electrospun solution was stabilized at 1 mL/h. Here, PLLA without addition of GEM was used as control. Next, the TA-mediated in-situ AgNP generation on the surface of electrospun fibers was achieved by simple two-step dipping strategy. First, the asprepared electrospun membranes were immersed in the 60% (w/w) TA aqueous solution for 24 h with constant stirring to facilitate adequate infiltration of TA molecules. After drying, the TA- treated membranes were dipped into silver nitrate aqueous solution (20 mg/mL) at room temperature overnight to enable insitu production of AgNPs on the PLLA fiber surface. Then, the obtained GEM@PLLA-TA- Ag membranes were rinsed with deionized water to remove the excessive uncoated AgNPs and stored at 4 ◦C for further experiments.

2.2. Characterization of the anti-bacterial and anti-cancer electrospun fibrous scaffolds

The morphology of electrospun membranes was examined by scanning electron microscopy (SEM) (Tescan VEGA3, Czech Republic). The samples were sputter-coated with gold before observation. Subsequently, the equipped energy dispersive X-ray spectroscopy (EDS) was used to assess their element composition. The specific chemical bonding was assessed by Fourier transform infrared (FTIR) (Thermo Nicolet iS5, US). In addition, we performed uniaxial tensile tests to analyse the mechanical performances of the fabricated membranes (50 mm length × 10 mm width × 0.2 mm thickness) using a mechanical tester (Instron, US). To obtain the stress-stain curve, the samples were subsequently stretched longitudinally at a speed of 5 mm/min until failure (n = 4).
Biomaterials Advances 137 (2022) 2128313

2.3. In vitro GEM release

The fibrous membrane samples with round shape (φ = 25 mm, total mass ≈70 mg) were immersed in a 15 mL centrifugal tube containing 5 mL PBS (phosphate-buffered saline, pH 7.4). After incubation for different time periods (0, 2, 8, 12, 24, 36, 48 h, 4, 7, 10, 14, 18, 24 and 30 days), 1.0 mL supernatant was collected from the centrifugal tubes for analysis, while 1 mL fresh PBS was supplemented into the centrifugal tube. Then, high-performance liquid chromatography (HPLC) was adopted to measure the quantity of released GEM in the supernatant. The detailed parameters were showed as follow: a mixed solution of ammonium acetate buffer (0.05 mol/L) and methanol (90:10, v/v %) was used as the mobile phase, flow rate was fixed at 1 mL/min, the detection wavelength was 268 nm, C18 column (50 mm × 4.6 mm for length, 5 μm for filler size) was used in the test with temperature at 30◦C.

2.4. Biocompatibility test

The biocompatibility of PLLA, PLLA-TA, and PLLA-TA-Ag mem- branes were evaluated by live/dead staining. Briefly, leaching solutions of different samples were prepared by incubating them in the complete culture medium for 24 h at 37 ◦C. PANC-1 (human PC cell line, Chinese Academy of Sciences) or NIH/3T3 cells (cell lines of mouse embryonic fibroblasts, ATCC® CRL-1658TM) were seeded at a cell density of 1 × 104 cells/cm2 and cultured overnight, and then we added 1 mL extract to each well and cultured the cells for 1, 3 and 5 days. Subsequently, the live/dead staining (Thermo Fisher, Hong Kong) was performed following the manufacture's protocol to evaluate cell viability.

2.5. Cell morphology

The cell morphology of PANC-1 and NIH/3T3 on the scaffolds was observed by F-actin staining. After complete sterilization of samples by ethanol and UV irradiation, the cells were seeded onto the membrane at a cell density of 1 × 104 cells/cm2. After culture for 1 day, samples were rinsed with PBS and fixed using 4% paraformaldehyde for 20 min, followed by staining with intracellular filament F-actin (phalloidin, Alexa Fluor 488, Thermo Fisher, Hong Kong) and cell nuclei (4 ´ ,6-Diamidino- 2-phenylindole dihydrochloride, DAPI, Thermo Fisher, Hong Kong) according to the manufacturer's instructions. Finally, the samples were observed using a confocal microscopy (Leica TCS SPE Confocal Microscope).

2.6. Anti-tumor effects of GEM-loaded membranes

The tumor-killing ability of the GEM-loaded membranes was evaluated by live/dead staining. Briefly, PANC-1 and NIH/3T3 were seeded at a cell density of 1 × 104 cells/cm2. After 1-day culture, the extracts of different samples were added to each well and co-cultured for 1, 3 and 5 days. Subsequently, cell viability was assessed by the live/dead staining (Thermo Fisher, Hong Kong). To evaluate the long-term anti-cancer properties, we treated PANC-1 cells with the extracts from the samples after 30-day incubation in PBS. Briefly, after incubation in PBS for 30 days, the samples were rinsed thoroughly and added with complete culture medium to prepare leaching solution. After co-culture of PANC-1 cells with leaching solution for 3 days, live/dead staining was performed to evaluate cell viability. The ratio of live cells to total cells, i.e., cell viability, was calculated via ImageJ software. Furthermore, cell proliferation was revealed by cell counting kit-8 (CCK-8) analysis, following the manufacturer's instruction. In brief, CCK-8 solution was added at a 10% volume of culture medium. After 4-h treatment, the absorbance at 450 nm was measured by a microplate reader.

2.7. Ant-bacterial test

In vitro anti-bacterial assessment of different samples was assessed against Citrobacter freundii (C. freundii, CGMCC 1.12847) using the colony counting method. C. freundii is a representative member of the Enterobacteriaceae family in the class of Gammaproteobacteria, which is a known cause of significant opportunistic infections and highly correlated to poor prognosis and immune dysregulation of patients with PC [22,23]. Briefly, bacterial cells were cultured in Mueller-Hinton broth for 24 h in a 37 ◦C incubator with 100 rpm in a shaker. Then, 0.5 mL of bacterial suspension (1 × 106 CFU/mL) were spread onto the samples and incubated for another 24 h at 37 ◦C. The bacterial suspension without treatment with samples was set as the control group. Then, 2 mL PBS was added to each group and kept shook for 20 min to resuspend the live bacteria. After a series of dilution, the bacterial suspension was spread onto the Luria-Bertani agar plates. The number of colonies on the Luria-Bertani agar plates was finally counted after 24-h culture.

2.8. In vivo inhibition effect of tumor recurrence

All animal experimental protocols were approved by the Ethics Committee of the Hong Kong Polytechnic University and Southwest Jiaotong University. Tumor model was established by subcutaneously inoculated

approximately 1 × 107 PANC-1 cells into the left side of the nude mice's back (n = 4) [14]. Mice were randomly divided into four groups including control, GEM, PLLA-TA-Ag and GEM2@PLLA-TA-Ag groups. When the tumor volume increased to 100 mm3, a small inci- sion was made on the mice skin and removed three-quarters of the tumor. For PLLA-TA-Ag and GEM2@PLLA-TA-Ag groups, 1 × 1 cm electrospun fibrous membranes were implanted into the residual tumor site after surgery. For the control and GEM groups, saline and GEM (100 mg/kg) were intraperitoneally injected respectively twice a week. Afterwards, the mice weight and tumor size were recorded every two days. The tumor size (V) was calculated following the equation: V = (length × width2) / 2.

2.9. Histological examination

At day 14, all mice were euthanized, and the residual tumor tissues were collected, scaled, and photographed. Then, these tumor tissues were fixed in 4% formaldehyde, dehydrated with gradient ethanol, embedded in paraffin blocks, cut into sections with 5-μm thickness, and stained with hematoxylin and eosin (H&E) (Beyotime, China) for microscopic observation. To better understand the anti-tumor efficacy of our membrane, immunohistochemical analysis was then conducted by incubating tumor slices with the rabbit polyclonal antibodies such as Ki- 67, B-cell lymphoma-2 (Bcl-2), and cleaved caspase-3 (Abcam, UK). After staining, an optical microscope (Olympus, Japan) was used to observe and photograph. Semi-quantitative analysis of immunohistochemical staining results was carried out according to previously published literature [14,24].

2.10. Statistical analysis

All experiments were conducted in triplicate if not specified. Data were displayed as mean ± standard deviation (SD) and analyzed by SPSS Statistics 17.0. (IBM Corp., USA). The one-way analysis of variance (ANOVA) test followed by Tukey's multiple comparison was carried out to identify between-group difference. Statistically significant differences were indicated by *$p < 0.05$, **$p < 0.01$ and ***$p < 0.001$.

3. Results and Discussion

3.1. Preparation and characterization of electrospun fibrous scaffolds

To prepare AAFM, we firstly fabricated the GEM-loaded PLLA electrospun fibrous scaffolds by blending electrospinning. As showed in Fig. 2A, all membranes showed continuous, uniform and smooth fibrous morphology, resembling the structure of native extracellular matrix (ECM). EDS analysis further confirmed the successful incorporation of GEM in the PLLA fibers. Additionally, we found although the addition of GEM significantly decreased the average fiber diameter of the membranes, no significant difference was found among GEM-containing membranes (Fig. 2B). Next, we used TA as the reducing agent stabilizer to modify the fiber surface, which endowed the membranes with excellent anti-bacterial performance by in-situ synthesis of AgNPs on the fibers. Due to the high specific surface area of electrospun fibers, our prepared membranes were believed to facilitate the TA-mediated AgNP reduction process. As expected, SEM observation and EDS analysis revealed a large number of AgNPs anchored on the fibers, both on the membrane surface and in the inner layer of membranes (Fig. 2A). Moreover, the fiber structure of GEM2@PLLA-TA-Ag was similar to that of GEM2@PLLA, indicating such two-step modification process did not compromise the fiber morphology. Most importantly, the highly porous structure remained in the resultant membranes after modification, which was beneficial for adequate cell contact. Later, the surface chemical composition of our prepared AAFM was analyzed by FTIR. As illustrated in Fig. 2C, the FTIR spectrum of GEM-containing samples exhibited the stretching vibration peaks of C– O at 1636 cm− 1 and 1750 cm− 1. With increase of the GEM content, the intensity of absorption peak at 1636 cm− 1 was enhanced, which suggested the feasibility of GEM encapsulation by blending electrospinning. In addition, compared

with original PLLA fibers, neither new peak nor peak shift was found in the FTIR spectra of PLLA-TA fibers (Fig. 2D). However, after the in-situ AgNP synthesis, the intensity of broad -OH band at around 3100–3600 cm− 1 was increased in the PLLA-TA-Ag group, which might be due to the formation of hydrogen bonding between TA and AgNP and/or between PLLA and AgNP. In addition, the van der Waals and electrostatic interactions between AgNP (positive charge) and the hydroxyl groups of PLLA (negative charge) might be another reason causing the increased peak intensity [25]. Moreover, we observed an obvious carbonyl peak shift from 1746 cm− 1 in PLLA to 1752 cm− 1 in PLLA-TA-Ag, which indicated the interaction of AgNPs with carbonyl groups in PLLA or oxidized TA. Altogether, these results demonstrated our AAFM were prepared successfully by facile blending electrospinning and TA- mediated two-step dipping.

As an artificial graft for in-situ implantation to suppress tumor recurrence, our proposed AAFM should possess appropriate mechanical performance, which can avoid unintended damage to surrounding tissues while facilitating the surgical operations. Thus, we evaluated the mechanical properties of different PLLA electrospun membranes via tensile stress-strain measurements. Our results revealed that after incorporation of GEM into PLLA, the mechanical properties such as tensile strength, extensibility and tensile modulus significantly decreased (Fig. 2E and F). Moreover, we found the mechanical properties of GEM2@PLLA-TA-Ag were slightly inferior to those of GEM2@PLLA, indicating that the TA-mediated two-step surface modification could potentially compromise the mechanical performances of the membranes possibly due to the influence of in situ reduction of AgNPs during the dipping process. However, the physical strength and stretchability of GEM2@PLLA-TA-Ag were still strong enough to satisfy the requirements of clinical applications that were served as a tissue filler after local resection of the PC tissue.

Subsequently, we investigated the GEM release from the PLLA electrospun fibers containing different content of GEM. It was revealed that the GEM release rate significantly increased in the PLLA fibers incorporating higher amount of GEM, indicating a controllable release profile (Fig. 2G). In addition, despite a remarkable burst GEM release at initial 36 h in GEM1@PLLA (37.33 ± 5.07%), GEM2@PLLA (47.08 ± 6.61%) and GEM3@PLLA (53.17 ± 6.13%) groups, a long-term GEM release pattern over two weeks was found among these groups thereafter. The GEM release from PLLA fibers was mainly through free diffusion along with the bulk degradation of PLLA. The initial burst GEM release was possibly due to the rapid GEM diffusion from the PLLA fibers upon immersing them in water, while the long-term release behavior might be attributed to the hydrophobic nature and slow degradation rate of PLLA [15]. Moreover, we found after TA-mediated surface modification, the GEM release rate was further decreased. The total cumulative GEM release amount of GEM2@PLLA-TA-Ag was 21.2 ± 5.45% within the initial 36 h, markedly lower than that of the GEM2@PLLA group. The further extended GEM release for GEM2@PLLA-TA-Ag might be resulted from the formation of TA-Ag complexes on PLLA fibers, which could act as a physical barrier to increase the GEM diffusion route into the surrounding solution. In short, the rapid GEM release from AAFM (i. e., GEM2@PLLA-TA-Ag) may be advantageous for the elimination of locally residual tumor cells after surgery, while the subsequent prolonged drug release pattern may mitigate the risk of later-stage cancer

recurrence.

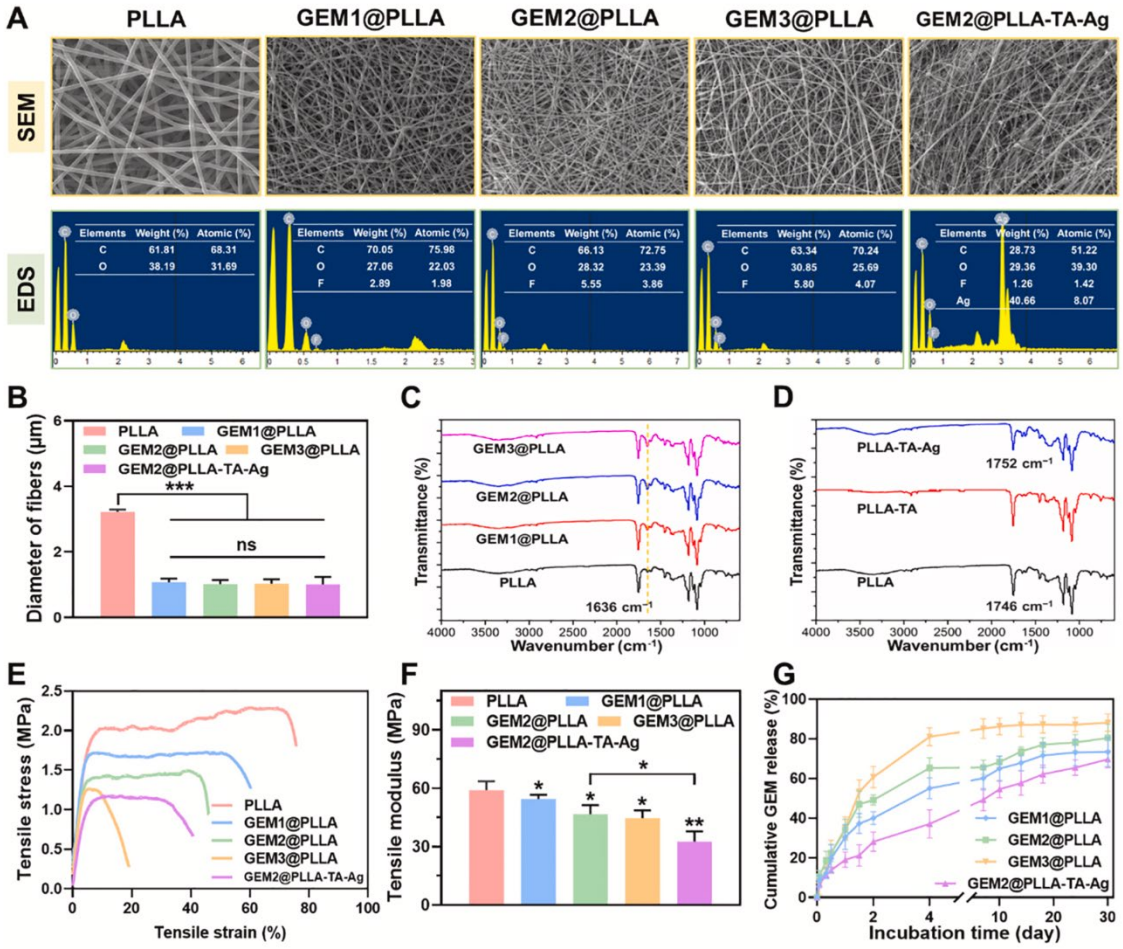

Fig. 2. Morphology and characterization of AAFM. (A) Representative SEM images and EDS results of different GEM-loaded electrospun scaffolds. (B) Corresponding average fiber diameter obtained based on the SEM images. FTIR spectra of (C) GEM-loaded fibrous membranes and (D) PLLA membranes with TA-mediated two-step modification treatment. (E) Representative tensile stress-strain curves and (F) corresponding tensile modulus of different electrospun fibers obtained by uniaxial tensile test. (G) Cumulative GEM release percentage. Data were expressed as mean ± SD (*$p < 0.05$, **$p < 0.01$ and ***$p < 0.001$).

3.2. In vitro cytotoxicity and anti-bacterial performance

In the PC microenvironment, cancer-associated fibroblasts (CAFs) are the most abundant population of stromal cells [26,27]. They play critical roles in PC progression such as promoting tumor cell proliferation and metastasis and secreting a large amount of ECM proteins to serve as a barrier to the penetration of chemo- and immuno-therapeutics [28–31]. Consequently, it might be a promising strategy to enhance the therapeutic effects by simultaneously eliminating CAFs and tumor cells. To preliminarily explore whether our delivery system (i.e., non-GEM
loaded membranes) could influence the growth of CAFs and tumor cells, we used NIH/3T3 (a cell line of mouse embryonic fibroblasts) and PANC-1 (a human PC cell line) as the model cells. Live/dead staining was first performed to investigate their in vitro cytotoxicity. Our results showed that there were many living NIH/3T3 and PANC-1 cells (stained green with calcein-AM) in the control, PLLA and PLLA-TA groups (Fig. 3A and B). Quantitation analysis further confirmed that the cell viability was similar among these three groups, which suggested their excellent in vitro biocompatibility (Supporting Information Fig. S1 and S2). However, in the PLLA-TA-Ag group, both NIH/3T3 and PANC-1 exhibited a significantly reduced cell viability during culture. Almost all NIH/3T3 and PANC-1 cells died (stained red with ethidium homodimer-

1) at day 3 and day 5, respectively (Fig. 3A and B). These results demonstrated the PLLA-TA-Ag displayed remarkable detrimental effects on the growth of NIH/3T3 and PANC-1 cells, indicating its synergistic cytotoxicity in tumor cells and CAFs. Since our facile two-step modification strategy was conducted in aqueous solution at room temperature without involvement of any organic solvent, such phenomenon might be attributed to the oxidative stress induced by AgNPs, which may induce cell damage by generation of reactive oxygen species (ROS). In addition, autophagy and apoptosis might be involved in this progress.
Cell morphology change was associated with cell function, and thus we further evaluated the cell morphology adhered onto different elecrospun membranes by actin/DAPI staining. As revealed in Fig. S3, cells on the PLLA and PLLA-TA groups showed similar morphology; that is, the NIH/3T3 showed a shuttle shape while PANC-1 exhibited a polygonal shape. However, compared with PLLA group, much more cells were attached on the PLLA-TA and cells showed slightly larger spreading area. This better cell adhesion in PLLA-TA could be explained by the increased hydrophilicity of TA modification. Moreover, the increased protein adsorption mediated by TA as well as the direct interaction between cell membrane and TA coating might be other potential reasons [32]. Notably, few cells were adhered onto PLLA-TA-Ag, and both NIH/3T3 and PANC-1 were not fully outspread with less pseudopodia extension. This result was consistent with that of the above live/dead staining, indicating that the generated AgNPs can inhibit cell growth. In terms of these unique performances of PLLA-TA-Ag, it could be hypothesized that after in vivo implantation into tumor resection site, the modified TA on PLLA-TA-Ag could rapidly recruit the surrounding residual cancer cells or fibroblasts to the scaffolds, and then the reduced AgNPs would efficiently suppress or even kill these cells, which coordinately enhanced the anti-cancer effects. Taken these results together, our PLLA-TA-Ag delivery platform could work synergistically with the cargoes (GEM)-dominated chemotherapy to effectively improve the postoperative outcomes following PC surgery.

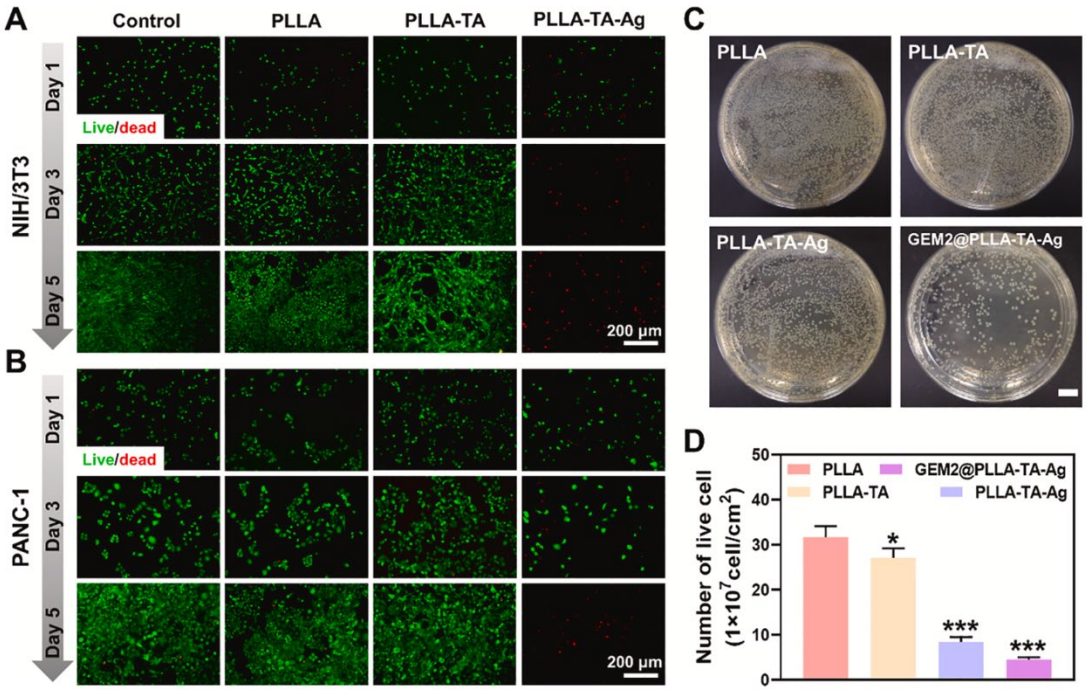

Fig. 3. In vitro biocompatibility and anti-bacterial performance of GEM delivery system (i.e., PLLA-TA-Ag). Live/dead staining of (A) NIH/3T3 and (B) PANC-1 cells by co-culture with the scaffold leaching solution for 1, 3 and 5 days. Green and red fluorescence indicate the live cells and dead cells, respectively. (C) Photographs of plates showing the anti-bacterial effects of different electrospun membranes against Citrobacter freundii. (D) Relative bacterial viability of Citrobacter freundii after contact with different electrospun membranes for 24 h. Scale bar = 1 cm. Data were expressed as mean ± SD (*$p < 0.05$ and ***$p < 0.001$). (For interpretation of the references to colour in this figure legend, the reader is referred to the web version of this article.)

Surgical site infection, caused by the common Gram-negative bacteria (e.g., E. coli) and Gram-positive bacteria (e.g., Enterococcus faecal), is highly related with the increased morbidity and mortality rate after

pancreatoduodenectomy [16,33]. Since the broad-spectrum antibacterial activities against E. coli and Enterococcus faecal by AgNPs or TA have been extensively documented in previous research [34–38], we have reasons to believe that our PLLA-TA-Ag could combat these bacteria and prevent the postoperative infection. Besides, previous studies have re- ported the Gammaproteobacteria, the most prevalent bacteria in the tumor microenvironment of PC, could diminish the chemotherapeutic efficacy of GEM by secreting cytidine deaminase to convert GEM into inactive form, 20,20-difluorodeoxyuridine [18]. Here, we used C. freundii., a representative member of the Enterobacteriaceae family in the Gammaproteobacteria class, as the model bacteria with a focus on investigating the ability of PLLA-TA-Ag to inhibit Gammaproteobacteria growth and teliminate Gammaproteobacteria-induced GEM resistance. It was revealed that colonies of Citrobacter freundii on agar plates of PLLA- TA-Ag and GEM2@PLLA-TA-Ag groups were significantly less than that of PLLA and PLLA-TA group after direct contact with different membranes for 24 h (Fig. 3C). Quantitative analysis further verified that GEM2@PLLA-TA-Ag group exhibited the most excellent anti-bacterial effects as compared with other groups (Fig. 3D). We speculated such outstanding anti-Gammaproteobacteria capacity could be mainly ascribed to the inherent antibacterial activity of the in-situ synthesized AgNPs, which have been demonstrated to combat bacteria by inducing denaturation of cell membranes or generating the ROS [39,40]. These results implied that the PLLA membrane modified with TA/AgNP deposition could prevent surgical site infection and improve the effectiveness of GEM-based chemotherapy by suppressing the Gammaproteobacteria growth.

3.3. In vitro anti-tumor activity

To assess the anti-tumor effects of different GEM-loaded fibrous membranes, we detected their in vitro inhibitory effects on the growth of tumor cells and fibroblasts via live/dead staining. As displayed in Fig. 4A and B, there were some live NIH/3T3 and PANC-1 cells in the GEM1@PLLA group after culture for 1 day. However, almost all cells died at day 3 and day 5. For GEM2@PLLA, GEM3@PLLA and GEM2@PLLA-TA-Ag, a large number of dead cells was found even after only 1-day culture, suggesting their superior potential for rapid removal of residual tumor cells and surrounding fibroblasts. Such excellent tumor-killing effects for GEM-loaded PLLA membranes could be attributed to the rapid GEM diffusion from fibers that caused the transient high drug concentration in the local cell microenvironment. For GEM2@PLLA-TA-Ag, the synergetic inhibition ability against NIH/3T3 and PANC-1 cells by TA/AgNP complexes on fiber surface could be another mechanism for the amplified anti-cancer effects. Subsequently, we evaluated the long-term inhibition effects of these GEM-loaded membranes on tumor cell growth. Different membranes were incu-bated in PBS solution for 30 days, and then their leaching solution was prepared to treat PANC-1 cells. After treatment for 3 days, we performed live/dead staining assay to examine the cell viability. Our results showed that compared with the control group, more red-labelled dead cells appeared in the GEM-loaded groups, and their PANC-1 cell viability was relatively reduced (Fig. 4C and D). Of note, GEM2@PLLA-TA-Ag exhibited lowest cell viability among these groups, indicating its superior inhibitory effect on PANC-1 cells. Then, we further assessed cell proliferation of PANC-1 cells after treatment with different membranes for 3 days by CCK-8 assay. Similarly, the results revealed more obvious inhibition effect of GEM2@PLLA-TA-Ag on PANC-1 cell proliferation (Fig. 4E). Altogether, these results collectively demonstrated our AAFM possessed a combined short- and long-term anti-cancer ability, showing great potential in suppressing cancer recurrence.

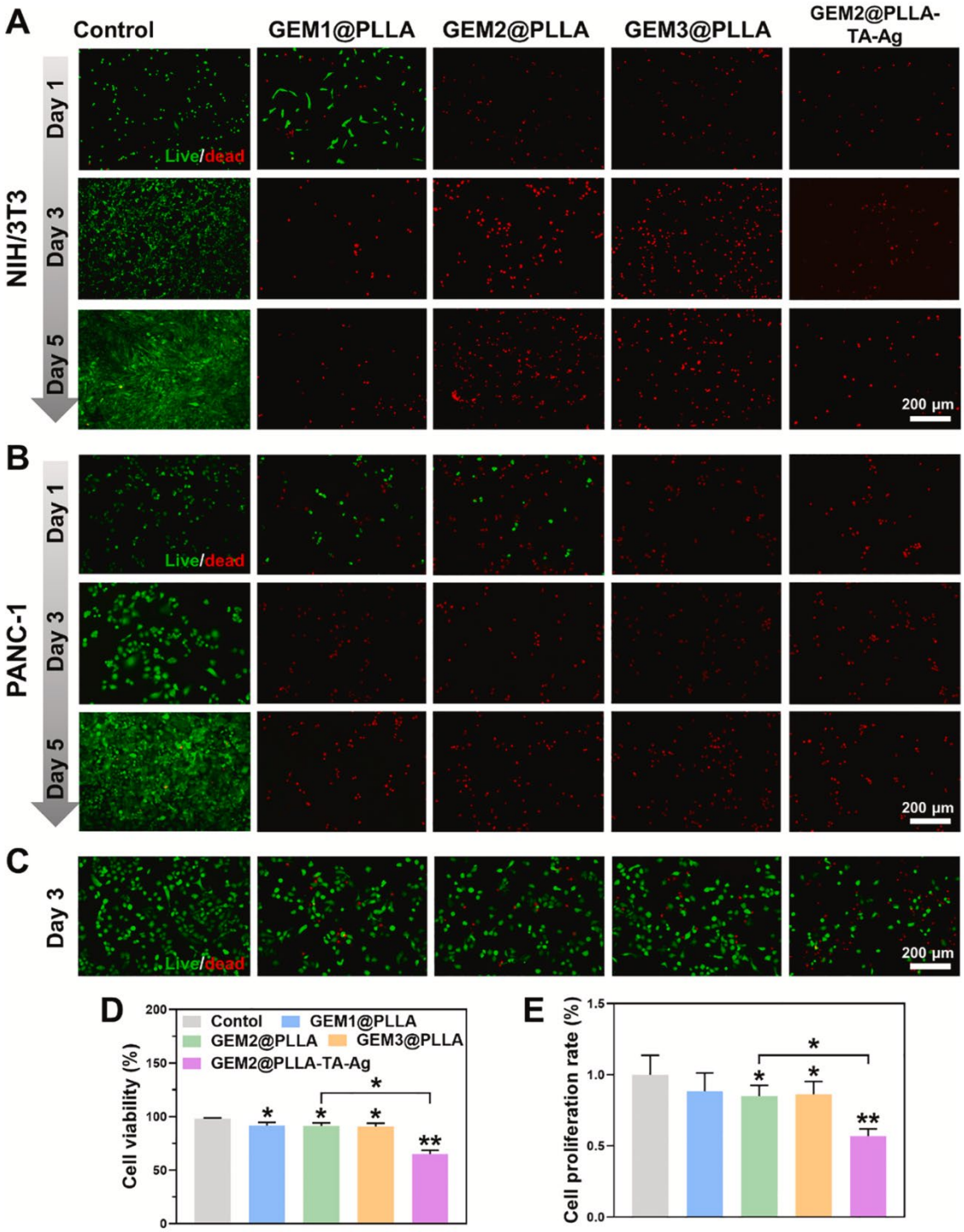

Fig. 4. In vitro anti-cancer efficiency of AAFM. Cytotoxicity evaluation of different electrospun membranes by co-culture of (A) NIH/3T3 and (B) PANC-1 cells with scaffold leaching solution for 1, 3 and 5 days. (C-E) Assessment of long-term anti-cancer performance of different electrospun membranes. (C) Live/dead staining of PANC-1 cells after treatment with the extracts from the samples after 30-day incubation in PBS. (D) Corresponding cell viability of PANC-1 cells quantitatively analyzed according to live/dead staining. (E) Proliferation analysis of PANC-1 cells by CCK-8 assay. Data were expressed as mean ± SD (*$p < 0.05$ and **$p < 0.01$).

3.4. In vivo anti-tumor recurrence ability

With the in vitro anti-bacterial and anti-cancer properties established, we proceed to evaluate the in vivo anti-tumor recurrence capability of our AAFM. In this study, a residual xenograft tumor model was created by subcutaneously injecting PANC-1 cells in nude mice. Then, normal saline (control) group, systemic GEM administration group, PLLA-TA-Ag implanted group and GEM2@PLLA-TA-Ag implanted group were set. As showed in Fig. 5A, our prepared electrospun membrane could be readily implanted onto tumor resection bed during surgery, indicating its feasible clinical application. After treating for 14 days, the photographs of the residual tumor from sacrificed mice showed that the size of solid tumor was smallest in GEM2@PLLA-TA-Ag, indicating its superior anti- tumor efficacy over that of other three groups (Fig. 5B). The variation of tumor volume also revealed that the recurrent tumor volume of the systemic GEM administration group was inhibited to some extent owing to the good anti-tumor activity of GEM (Fig. 5C). Surprisingly, we found the PLLA-TA-Ag exhibited better tumor inhibition effect than the systemic GEM administration group, possibly due to the cytotoxic effects of the anchored AgNPs. Of particular note, GEM2@PLLA-TA-Ag group achieved the most effective inhibition effect on tumor recurrence (mean tumor volume ≈52 mm3 at day 14), which attributed to the synergistic multi-step cell growth inhibition and local anti-bacterial therapy. Similarly, the average weight of the residual tumor also confirmed the excellent anti-recurrence efficiency of GEM2@PLLA-TA-Ag (Fig. 5D). It was also found that there was almost no significant change in the body weight of mice in GEM2@PLLA-TA-Ag, suggesting a low systemic toxicity caused by local and sustained drug release. Subsequently, the anti-recurrence performance of different treatments was further assessed by the histological analysis of the excised tumor tissues. As observed in H&E staining images, tumor slices of GEM and PLLA-TA-Ag groups showed more obvious nuclei fragmentations and void spaces as compared to the control group. Among these groups, GEM2@PLLA-TA- Ag presented most significant cell nuclei lysis and membrane destruction, suggesting that tumor tissue has undergone apoptotic and necrotic changes.

Additionally, we performed the immunohistochemical analysis of tumor region to investigate the underlying mechanism of tumor killing effect (Fig. 6). Bcl-2 is a cell survival protein that plays a key role in inhibiting programmed cell death and apoptosis and is closely correlated to chemoresistance [41,42]. Ki-67 is a cell proliferation index associated with the prognostic outcomes in PC [43], while cleaved-caspase3, the activated form of caspase3, is a pro-apoptosis protein that manipulates stress-related cell death [44]. Here, we evaluated the expression levels of these three markers in tumor tissues by immunohistochemical staining. As expected, Bcl-2 and Ki-67 expressions were significantly reduced but cleaved-caspase3 was remarkably increased in systemic GEM adminis- tration and PLLA-TA-Ag groups, compared with the control groups (Fig. 6A and B). The GEM2@PLLA-TA-Ag-treated tumor section exhibited the lowest Bcl-2 and Ki-67 levels and the highest cleaved- caspase3 level. All these results validated that our AAFM could effec- tively suppress the tumor growth by inducing tumor cell apoptosis and hampering cell proliferation in vivo. We speculated that the sustained GEM delivery from AAFM to the surgical site could rapidly kill the re- sidual tumor cells to ensure long-term therapeutic efficacy while avoiding the side effects resulted from GEM burst release. Meanwhile, the GEM delivery platform (i.e., PLLA-TA-Ag) could exert synergistic anti-tumor effect in vivo by its surface-attached TA/AgNP complexes, thereby markedly inhibiting tumor recurrence.

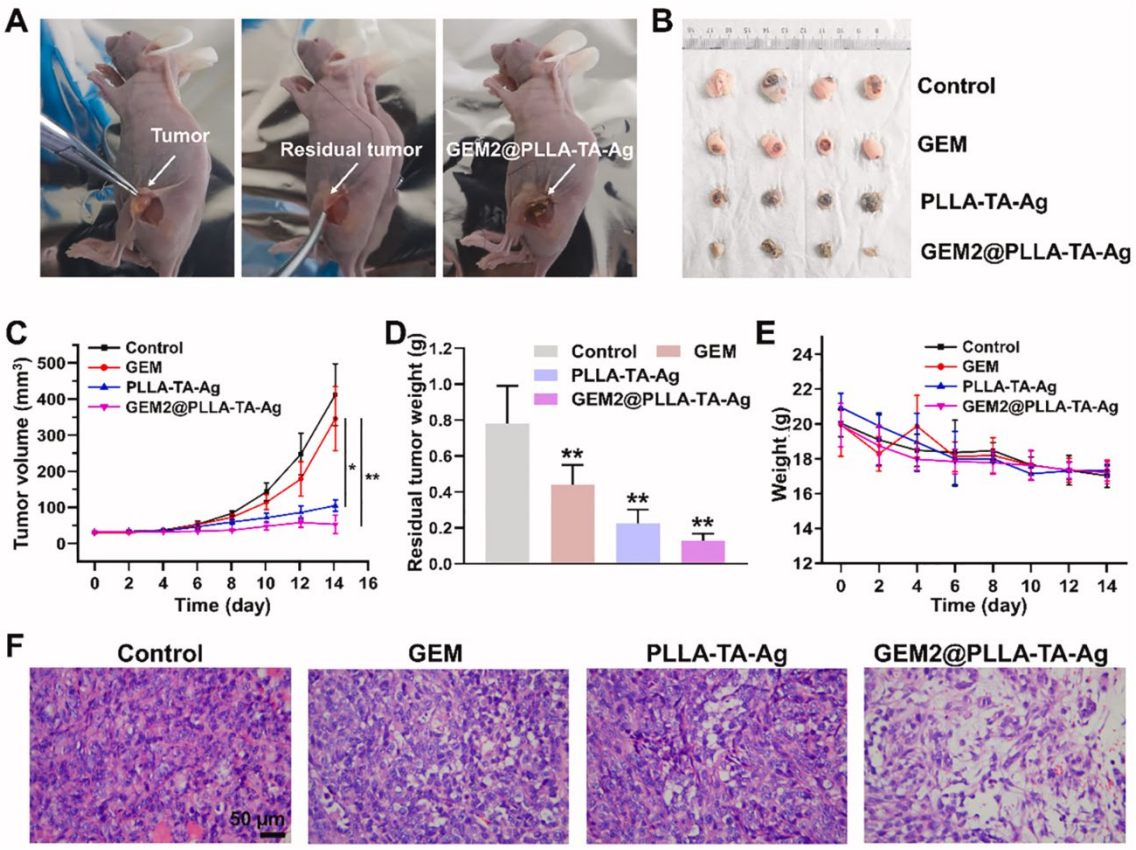

Fig. 5. In vivo anti-recurrence effect of AAFM in PANC-1 cell tumor-bearing mice. (A) Photographs showing the implantation of GEM2@PLLA-TA-Ag in residual tumor of nude mice for local therapy. (B) Photographs of residual tumor of PC (n = 4). (C) Changes of the tumor volume after treatment with different material formulations for 14 days. (D) Residual tumor weight of different groups. (E) Mouse weight of different groups. (F) H&E staining of the residual tumor after different treatment. Data were expressed as mean ± SD (*$p < 0.05$ and **$p < 0.01$).

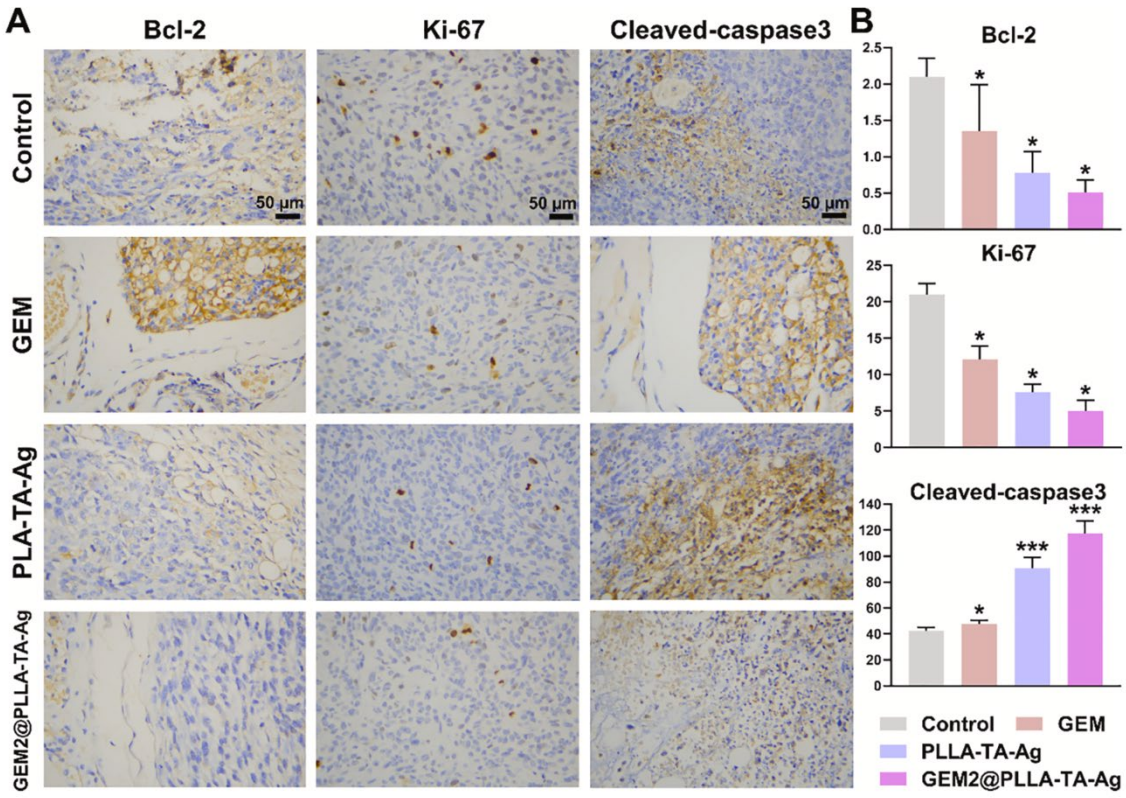

Fig. 6. (A) Immunohistochemical staining of Bcl-2, Ki-67 and cleaved-caspase3 of tumor sections at day 14. (B) Semi-quantitative analysis of the expressions of Bcl-2, Ki-67, and cleaved-caspase3. Data were expressed as mean ± SD (*$p < 0.05$ and ***$p < 0.001$).

4. Conclusion

In summary, we have successfully prepared an electrospun fiber, AAFM, with anti-cancer and anti-bacterial performance by blending electrospinning of GEM and PLLA and subsequent TA-mediated two-step in-situ AgNP deposition. This facile but delicate design not only harmonized favourable fibrous architecture and appropriate mechanical equipped it with multiple synergistic anti-tumor effects; that is, the surface modified TA/AgNP complexes could (1) prolong the GEM release to facilitate long-term inhibition of cancer recurrence, (2) combat the pathogenic microorganisms to prevent surgical site infection and mitigate Gammaproteobacteria-induced GEM resistance, and (3) kill the cancer cells to strengthen the efficacy of GEM-based adjuvant chemo- therapy. Compared with other systems for post-surgical cancer therapy [4,14], our AAFM possesses many unique advantages including facile and labour-saving preparation process, low-cost component materials, easy storage, and ready-to-use nature without involvement of any biological agents, etc. Taken together, this study provides a proof-of- concept demonstration of the combined anti-cancer and anti-bacterial strategy to effectively enhance the efficacy of postoperative adjuvant chemotherapy and prevent cancer recurrence.

CRediT authorship contribution statement

Qiang Zhang: Conceptualization, Methodology, Investigation, Data analysis, Writing – original draft. **Yang Luo**: Methodology, Investigation, Data analysis, Writing – original draft. **Bo Liang**: Methodology, Investigation, Data analysis. **Di Suo**: Methodology, Investigation, Data analysis. **Shang Lyu**: Methodology, Investigation, Data analysis. **Yi Wang**: Supervision, Resources, Manuscript revision. **Xin Zhao**: Conceptualization, Supervision, Resources, Manuscript revision.

Declaration of competing interest

The authors declare no competing financial interest.

Acknowledgements

This work was supported by the General Research Scheme (15202119) of the Research Grants Council of Hong Kong and the Sichuan Science and Technology Program of Sichuan Province

Appendix A. Supplementary data

Supplementary data to this article can be found online at https://doi. org/10.1016/j.bioadv.2022.212831.

References

[1] J.D. Mizrahi, R. Surana, J.W. Valle, R.T. Shroff, Pancreatic cancer, Lancet 395 (10242) (2020) 2008–2020.

[2] R.L.Siegel,K.D.Miller,A.Jemal,Cancerstatistics,2020,CACancerJ.Clin.70(1) (2020) 7–30.

[3] T.Kamisawa,L.D.Wood,T.Itoi,K.Takaori,Pancreaticcancer,Lancet388(10039) (2016) 73–85.

[4] L.L.Bu,J.Yan,Z.Wang,H.Ruan,Q.Chen,V.Gunadhi,R.B.Bell,Z.Gu,Advances in drug delivery for post-surgical cancer treatment, Biomaterials 219 (2019), 119182.

[5] H. Zhang, S. Xu, J. Zhang, Z. Wang, D. Liu, L. Guo, C. Cheng, Y. Cheng, D. Xu, M. G. Kong, Plasma-activated thermosensitive biogel as an exogenous ROS carrier for post-surgical treatment of cancer, Biomaterials 276 (2021), 121057.

[6] T. Conroy, P. Hammel, M. Hebbar, M. Ben Abdelghani, A.C. Wei, J.-L. Raoul,L. Chon´e, E. Francois, P. Artru, J.J. Biagi, FOLFIRINOX or gemcitabine as adjuvant therapy for pancreatic cancer, N. Engl. J. Med. 379 (25) (2018) 2395–2406.

[7]T.Manabe,H.Okino,R.Maeyama,K.Mizumoto,E.Nagai,M.Tanaka,T.Matsuda, Novel strategic therapeutic approaches for prevention of local recurrence of pancreatic cancer after resection: trans-tissue, sustained local drug-delivery systems, J. Control. Release 100 (3) (2004) 317–330.

[8] X. Li, F. Xu, Y. He, Y. Li, J. Hou, G. Yang, S. Zhou, A hierarchical structured ultrafine fiber device for preventing postoperative recurrence and metastasis of breast cancer, Adv. Funct. Mater. 30 (45) (2020), 2004851.

[9] Y.H.Yun,B.K.Lee,K.Park,Controlleddrugdelivery:historicalperspectiveforthe next generation, J. Control. Release 219 (2015) 2–7.

[10] E. Katsuta, Q. Qi, X. Peng, S.N. Hochwald, L. Yan, K. Takabe, Pancreatic adenocarcinomas with mature blood vessels have better overall survival, Sci. Rep. 9 (1) (2019) 1–11.

[11] D. Mathios, J.E. Kim, A. Mangraviti, J. Phallen, C.-K. Park, C.M. Jackson,T. Garzon-Muvdi, E. Kim, D. Theodros, M. Polanczyk, Anti-PD-1 antitumor immunity is enhanced by local and abrogated by systemic chemotherapy in GBM, Sci. Transl. Med. 8 (370) (2016), 370ra180-370ra180.

[12] C. Wang, J. Wang, X. Zhang, S. Yu, D. Wen, Q. Hu, Y. Ye, H. Bomba, X. Hu, Z. Liu, In situ formed reactive oxygen species–responsive scaffold with gemcitabine andcheckpoint inhibitor for combination therapy, Sci. Transl. Med. 10 (429) (2018),eaan3682.

[13] J.A. Kaplan, R. Liu, J.D. Freedman, R. Padera, J. Schwartz, Y.L. Colson, M.W. Grinstaff, Prevention of lung cancer recurrence using cisplatin-loadedsuperhydrophobic nanofiber meshes, Biomaterials 76 (2016) 273–281.

[14] G. Xia, H. Zhang, R. Cheng, H. Wang, Z. Song, L. Deng, X. Huang, H.A. Santos,W. Cui, Localized controlled delivery of gemcitabine via microsol electrospun fibers to prevent pancreatic cancer recurrence, Adv. Healthc. Mater. 7 (18) (2018), 1800593.

[15] Q. Zhang, Y. Li, Z.Y.W. Lin, K.K. Wong, M. Lin, L. Yildirimer, X. Zhao, Electrospun polymeric micro/nanofibrous scaffolds for long-term drug release and their biomedical applications, Drug Discov. Today 22 (9) (2017) 1351–1366.

[16] Ç.Bilgiç,S ¸Keske,E.Sobutay,U.Can,S.Zenger,B.Gürbüz,O¨.Ergo¨nül,O.Bilge, Surgical site infections after pancreaticoduodenectomy: preoperative biliary system interventions and antimicrobial prophylaxis, Int. J. Infect. Dis. 95 (2020) 148–152.

[17] K. Okano, T. Hirao, M. Unno, T. Fujii, H. Yoshitomi, S. Suzuki, S. Satoi,

S. Takahashi, O. Kainuma, Y. Suzuki, Postoperative infectious complications after pancreatic resection, J. Br. Surg. 102 (12) (2015) 1551–1560.

[18] L.T. Geller, M. Barzily-Rokni, T. Danino, O.H. Jonas, N. Shental, D. Nejman,

N. Gavert, Y. Zwang, Z.A. Cooper, K. Shee, Potential role of intratumor bacteria in mediating tumor resistance to the chemotherapeutic drug gemcitabine, Science 357 (6356) (2017) 1156–1160.

[19] K.B. Stopa, A.A. Kusiak, M.D. Szopa, P.E. Ferdek, M.A. Jakubowska, Pancreatic cancer and its microenvironment—recent advances and current controversies, Int. J. Mol. Sci. 21 (9) (2020) 3218.

[20] F. McAllister, M.A.W. Khan, B. Helmink, J.A. Wargo, The tumor microbiome in pancreatic cancer: bacteria and beyond, Cancer Cell 36 (6) (2019) 577–579.

[21] Y. Bu, S. Zhang, Y. Cai, Y. Yang, S. Ma, J. Huang, H. Yang, D. Ye, Y. Zhou, W. Xu, Fabrication of durable antibacterial and superhydrophobic textiles via in situ synthesis of silver nanoparticle on tannic acid-coated viscose textiles, Cellulose 26 (3) (2019) 2109–2122.

[22] J. Chakladar, S.Z. Kuo, G. Castaneda, W.T. Li, A. Gnanasekar, M.A. Yu, E.Y. Chang, X.Q. Wang, W.M. Ongkeko, The pancreatic microbiome is associated with carcinogenesis and worse prognosis in males and smokers, Cancers 12 (9) (2020) 2672.

[23] C.-C. Kao, M.-F. Liu, C.-F. Lin, Y.-C. Huang, P.-Y. Liu, C.-W. Chang, Z.-Y. Shi, Antimicrobial susceptibility and multiplex PCR screening of AmpC genes from isolates of Enterobacter cloacae, citrobacter freundii, and Serratia marcescens, J. Microbiol. Immunol. Infect. 43 (3) (2010) 180–187.

[24] X. Huang, C. Ou, Y. Shu, Y. Wang, S. Gong, R. Luo, S. Chen, Q. Wu, C. Gong, A self- sustained nanoplatform reverses TRAIL-resistance of pancreatic cancer through coactivating of exogenous and endogenous apoptotic pathway, Biomaterials 272 (2021), 120795.

[25] S. Calamak, M. Ermis, In situ silver nanoparticle synthesis on 3D-printed polylactic acid scaffolds for biomedical applications, J. Mater. Res. 36 (1) (2021) 166–175.

[26] W.J. Ho, E.M. Jaffee, L. Zheng, The tumour microenvironment in pancreatic cancer—clinical challenges and opportunities, Nat. Rev. Clin. Oncol. 17 (9) (2020) 527–540.

[27] C. Qu, Q. Wang, Z. Meng, P. Wang, Cancer-associated fibroblasts in pancreatic cancer: should they be deleted or reeducated? Integr. Cancer Ther. 17 (4) (2018) 1016–1019.

[28] Y. Li, Z. Zhao, C.-Y. Lin, Y. Liu, K.F. Staveley-OCarroll, G. Li, K. Cheng, Silencing PCBP2 normalizes desmoplastic stroma and improves the antitumor activity of chemotherapy in pancreatic cancer, Theranostics 11 (5) (2021) 2182.

[29] F. Fan, L. Jin, L. Yang, pH-sensitive nanoparticles composed solely of membrane- disruptive macromolecules for treating pancreatic cancer, ACS Appl. Mater. Interfaces 13 (11) (2021) 12824–12835.

[30] S. Yachida, S. Jones, I. Bozic, T. Antal, R. Leary, B. Fu, M. Kamiyama, R.H. Hruban, J.R. Eshleman, M.A. Nowak, Distant metastasis occurs late during the genetic evolution of pancreatic cancer, Nature 467 (7319) (2010) 1114–1117.

[31] J. Norton, D. Foster, M. Chinta, A. Titan, M. Longaker, Pancreatic cancer associated fibroblasts (caf): under-explored target for pancreatic cancer treatment, Cancers 12 (5) (2020) 1347.

[32] K. Wu, X. Wu, J. Guo, Y. Jiao, C. Zhou, Facile Polyphenol–europium assembly enabled functional poly (l-lactic acid) nanofiber mats with enhanced antioxidation and angiogenesis for accelerated wound healing, Adv. Healthc. Mater. 10 (19) (2021), 2100793.

[33] T.K. Maatman, D.J. Weber, L.R. Timsina, B. Qureshi, E.P. Ceppa, A. Nakeeb, C. M. Schmidt, N.J. Zyromski, L.G. Koniaris, M.G. House, Antibiotic irrigation during pancreatoduodenectomy to prevent infection and pancreatic fistula: a randomized controlled clinical trial, Surgery 166 (4) (2019) 469–475.

[34] L. Liu, C. Ge, Y. Zhang, W. Ma, X. Su, L. Chen, S. Li, L. Wang, X. Mu, Y. Xu, Tannic acid-modified silver nanoparticles for enhancing anti-biofilm activities and modulating biofilm formation, Biomater. Sci. 8 (17) (2020) 4852–4860.

[35] S. Ahmed, M. Ahmad, B.L. Swami, S. Ikram, A review on plants extract mediated synthesis of silver nanoparticles for antimicrobial applications: a green expertise, J. Adv. Res. 7 (1) (2016) 17–28.

[36] H. Yousaf, A. Mehmood, K.S. Ahmad, M. Raffi, Green synthesis of silver nanoparticles and their applications as an alternative antibacterial and antioxidant agents, Mater. Sci. Eng. C 112 (2020), 110901.

[37] D. Wu, W. Fan, A. Kishen, J.L. Gutmann, B. Fan, Evaluation of the antibacterial efficacy of silver nanoparticles against enterococcus faecalis biofilm, J Endod. 40 (2) (2014) 285–290.

[38] B. Kaczmarek, Tannic acid with antiviral and antibacterial activity as a promising component of biomaterials-a minireview, Materials 13 (14) (2020) 3224.

[39] Y.Y. Loo, Y. Rukayadi, M.-A.-R. Nor-Khaizura, C.H. Kuan, B.W. Chieng,M. Nishibuchi, S. Radu, In vitro antimicrobial activity of green synthesized silver nanoparticles against selected gram-negative foodborne pathogens, Front. Microbiol. 9 (2018) 1555.

[40] S. Liao, Y. Zhang, X. Pan, F. Zhu, C. Jiang, Q. Liu, Z. Cheng, G. Dai, G. Wu, L. Wang, Antibacterial activity and mechanism of silver nanoparticles against multidrug- resistant Pseudomonas aeruginosa, Int. J. Nanomedicine 14 (2019) 1469.

[41] A. Adamska, O. Elaskalani, A. Emmanouilidi, M. Kim, N.B.A. Razak, P. Metharom, M. Falasca, Molecular and cellular mechanisms of chemoresistance in pancreatic cancer, Adv. Biol. Regul. 68 (2018) 77–87.

[42] H. Wang, R. Ren, Z. Yang, J. Cai, S. Du, X. Shen, The COL11A1/Akt/CREB signaling axis enables mitochondrial-mediated apoptotic evasion to promote chemoresistance in pancreatic cancer cells through modulating BAX/BCL-2 function, J. Cancer 12 (5) (2021) 1406.

[43] M. Jamali, R. Chetty, Predicting prognosis in gastroentero-pancreatic neuroendocrine tumors: an overview and the value of Ki-67 immunostaining, Endocr. Pathol. 19 (4) (2008) 282–288.

[44] X. Liu, Y. He, F. Li, Q. Huang, T.A. Kato, R.P. Hall, C.Y. Li, Caspase-3 promotes genetic instability and carcinogenesis, Mol. Cell 58 (2) (2015) 284–296.